High-electric-field transport in a-Si:H. I. Transient photoconductivity

C. E. Nebel, R. A. Street, and N. M. Johnson
Xerox Palo Alto Research Center, Palo Alto, California 94304

J. Kocka
Institute of Physics, Czechoslovak Academy of Sciences, 16200 Praha 6, Cukrovarnicka 10, Czechoslovakia
(Received 12 February 1992)

The drift mobility of electrons at low temperatures in amorphous hydrogenated silicon is investigated by time-of-flight and charge-collection measurements. The experiments performed on *p-i-n* junctions in the temperature range $40 < T < 200$ K reveal the strong influence of the electric field on carrier propagation. At 40 K, where thermally induced transport can be neglected, the drift mobility of electrons is enhanced by many orders of magnitude up to values of $\mu_D > 10^{-2}$ cm^2/V s. The mobility has a superlinear dependence on the electric field and shows a time and thickness dependence indicative of dispersive transport. The high-field $\mu\tau$ product measured at 40 K is three orders of magnitude larger than the low-field $\mu\tau$ product calculated from dc-photoconductivity experiments. A model of field-enhanced band-tail hopping is developed to interpret the data. We show that the electric field creates a quasimobility edge in the tail region at an energy level E_t which depends on the field strength and the tail state distribution. The hopping mobility as well as the energy level of the quasimobility edge are strongly dependent on the electric field. Ballistic capture of carriers into traps below the quasimobility edge is identified as the origin of dispersion. We introduce transport equations to calculate the drift of an ensemble of nonequilibrated carriers, and find reasonable agreement with experimental data assuming an exponential distribution of band-tail localized states with characteristic energy of 25 meV and localization length of $6 \leq \alpha \leq 9$ Å. We also discuss the introduction of an effective temperature as a substitute for the electric field.

I. INTRODUCTION

Amorphous hydrogenated silicon (*a*-Si:H) can be doped effectively,[1,2] and this property has attracted considerable interest and research efforts as well as applications in large-area electronics, solar cells, and thin film transistors. The electronic properties of *a*-Si:H are dominated by carrier interactions with the disorder-induced density of localized band-tail states in the gap adjacent to the conduction and valence bands. The mechanisms of carrier propagation depend sensitively on the temperature and the density of localized states, varying from transport in the bands of extended states to hopping in the distribution of localized states. With the increasing quality of *a*-Si:H, the application of sensitive transport experiments such as time of flight, dark conductivity, and photoconductivity have revealed a variety of phenomena.

The mobility of electrons and holes is rather small compared to crystalline silicon and decreases continuously at lower temperatures.[3–8] The drift mobility of a nonequilibrated ensemble of carriers is time dependent below 250 and 410 K for electrons[4–6] and holes,[7,8] respectively, and is referred to as dispersive transport. The drift mobility measured by time-of-flight experiments in the dispersive transport regime is a nonlinear function of the electric field F. However, the field dependence is a consequence of the time-dependent mobility and is not an intrinsic field dependence of the microscopic transport mechanism. Most of the transport phenomena have been explained within the framework of the multiple trapping model (MT) described by Schmidlin in 1977.[9] It is assumed that inelastic scattering[10] of moving carriers in the extended states occurs at nearly every atomic site and causes fast trapping into band-tail localized states below the mobility edge. The carriers are subsequently thermally reemitted back to the extended states. The time-dependent shift of the distribution of nonequilibrated carriers deeper into the band tail and the related decrease of the reemission rate is the origin of the dispersive transport property. The interaction of carriers with neighboring localized states through tunneling transitions (phonon-induced nearest-neighbor or variable range hopping), as well as temperature-induced shifts of the mobility edges, are neglected in the model. This restricts the application of the MT model to transport in the medium-temperature regime. The MT model also fails to explain the recent observations of electric-field-induced transport effects of *a*-Si:H.[11–18] Despite the increasing amount of data available in the literature, the high-field effects are not well understood and are controversial.

Several time-of-flight and conductivity experiments have observed enhancements of transport properties in the presence of high electric fields ($F > 8 \times 10^4$ V/cm).[11–18] The field effect is particularly strong at low temperatures where transport by the thermally induced multiple trapping mechanism can be neglected.[14,15,17,18] Measurements performed in the nondispersive temperature regime point towards a superlinear (Devlen, Tauc, and Schiff,[11] Imao, Nakajima, Nakata, Hattori, Shirafuji, and Inuishi[16]) or linear (Juska, Jukonis, and Kocka[13]) in-

crease of the drift mobility. Antoniadis and Schiff[12] were able to separate dispersion effects from nonlinear field-induced transport by using transient photoconductivity in conjunction with time-of-flight experiments. They deduced an exponential field dependence of the mobility where the field effect is increasing to the lower temperatures. Speculations about the origin of the enhancements include a field dependence of the microscopic mobility,[11,13] field-induced reemission of trapped carriers back into the conduction band,[12] and hot electrons.[16] It is interesting to note that the thermalization of carriers at high fields is reported to be field independent.[12]

Stachowitz, Fuhs, and Jahn[18] discovered a strong superlinear enhancement of the photoconductance which extends over several orders of magnitude at low temperatures. Surprisingly, small fields of the order $F > 3 \times 10^3$ V/cm lead to the onset of the field enhancement. The authors attributed the effect to a field-induced displacement of carriers during the thermalization in the band tails. Measurements of dc dark conductivity on doped *a*-Si:H (Nebel[17]) show comparable conductivity enhancements which support the model of field-induced hopping in the band tail. The highly superlinear increase of the conductivity with electric field agrees well with the mobility data deduced from time-of-flight experiments, and indicates a general change of transport properties in the tail region from multiple trapping to hopping.

A theoretical discussion of high-field transport in *a*-Si:H, presented by Shklovskii, Levin, Fritzsche, and Baranovskii[19] and Esipov,[20] develops two basic ideas. Shklovskii *et al.*[19] convert the electric-field effect into an effective temperature given by

$$T_{\text{eff}} = \frac{q\alpha F}{2k} , \tag{1}$$

where q is the elementary charge, α is the localization length, F is the electric field, and k is the Boltzmann constant, and apply the conventional transport equations[21] to derive the high-field transport. The effective temperature enters the distribution function of carriers (Boltzmann or Fermi-Dirac function). They argue that field-induced redistribution in the tail region accounts for the experimentally detected transport enhancements. This model, however, has several shortcomings. In addition to the field-induced change of the carrier distribution, it is likely that the hopping mobility is also field dependent and this effect is neglected in this model. Recent Monte Carlo simulations[22] and experimental data[17] do not support the hypothesis of a general equivalence between electric field and temperature. Both parameters should affect carrier propagation in different ways as the temperature is an isotropic and the field a vectorized quantity. We discuss this problem further in Sec. III of this paper. Esipov[20] includes tunneling from localized states to the mobility edge in the multiple trapping theory and successfully explains the transport data of Antoniadis and Schiff.[12] The model accounts for an exponential field dependence of the drift mobility and for the absence of field-dependent dispersion effects. However, these are opposite to the experimental data reported by Nebel and Kocka,[15] and Nebel.[17]

The coexistence of thermal- and field-induced transport in the medium-temperature regime ($T > 100$ K) creates several problems. There are experimental limitations like limited field strength, due to the moderate dark conductivity. Field- and thermally induced effects interact and are difficult to separate. The reported field-induced transport enhancements are therefore only in the range 2–10, which makes an analytical interpretation of the field dependence (exponential, superlinear, etc.) difficult. The investigation and understanding of field-dominated transport phenomena is the focus of this and the following companion paper and is a precondition on an analysis of the regime where thermal- and field-induced transport coexist. We therefore focus on the low-temperature regime where low-field multiple trapping transport is negligible. In the first paper the thermalization and propagation of electrons in the shallow region of the conduction-band tail is introduced and interpreted. In the second paper we focus on the propagation of deep trapped electrons and holes to complete the description and interpretation of field-induced transport features.

The first part is organized as follows. Section II describes electron transport and charge-collection data measured by time-of-flight experiments at $40 < T < 200$ K and at fields up to 5×10^5 V/cm on *a*-Si:H *p-i-n* junctions of different thicknesses. The low-temperature data are analyzed in Sec. III, based on a model of field-enhanced hopping in the tail states of the conduction band. The conclusions are related to the distribution of tail states, the localization length, and the establishment of a quasi-mobility edge in the presence of high electric fields. Section IV discusses the introduction of an effective temperature as a substitute for the field, based on electron mobility and dispersion data measured at high and low fields over a broad temperature regime.

II. TRANSIENT PHOTOCONDUCTIVITY AT HIGH ELECTRIC FIELDS

A. Experiment

Time-of-flight measurements in the temperature range $40 < T < 200$ K and at fields up to 5×10^5 V/cm were performed in order to determine the field and temperature dependence of the electron mobility. We use a conventional setup consisting of a high voltage pulse generator, a nitrogen pumped dye laser, a fast digitizing oscilloscope, and a cryostat.[23] The nonequilibrium electron density is created by a short laser flash of strongly absorbed light ($\lambda \simeq 530$ nm, absorption coefficient $\simeq 10^5$ cm^{-1}) from the laser, with a half pulse width of 3 ns. Measurements were carried out on reverse bias *p-i-n* junctions of thickness of 2 and 10 μm with thin (40 nm thick) phosphorus- and boron-doped layers as blocking contacts. The *p-i-n* junctions were deposited by conventional rf glow discharge of SiH_4 (for the intrinsic layer) and SiH_4/PH_3 or SiH_4/B_2H_6 mixtures (for n^+ and p^+ layers, respectively) with deposition parameters typical for high-quality *a*-Si:H. The delay time between applied field and laser excitation was shorter than 20 μs and the excitation level well below the level for space-charge distor-

tions ($Q_{exc} \leq 9 \times 10^{-10}$ A s). Transient currents were averaged over ten recordings with a period between pulses of 10 s. The collection efficiency was determined by charge-collection experiments with an absolute calibration by use of a c-Si photodiode. In order to record the transient signals over extended periods of time we applied a combined pulse technique[24] where the sensitivity of the detection system is increased continuously with decreasing signal amplitude.

B. Temperature- and field-dependent current decay

Figure 1 shows temperature-dependent electron transients recorded at fields of 3×10^5, 3.5×10^5, and 4×10^5 V/cm on the 10-μm *p-i-n* structure. The initial current decay (time $t < t_T$, where t_T is the transit time) is dominated by electron interactions with shallow traps, and is well described by a power-law time dependence,

$$I(t) \sim t^{-(1-\alpha_D)}, \tag{2}$$

where $I(t)$ is the current and α_D is the dispersion parameter. Dispersion of this form is a general feature of high-field transport and is also detected on the 2-μm sample. It is important to note that the displayed transients have been measured in the regime $50 < T < 160$ K where low-field transient currents approach $I \sim t^{-1}$ behavior.[25] The thermalization rate slows down for fields greater than 10^5 V/cm and α_D becomes strongly dependent on F. The field and temperature dependence of α_D are summarized in Fig. 2.

The low-field temperature dependence of α_D is well understood. A pure exponential tail state distribution results in a linear temperature dependence of α_D given by[23]

$$\alpha_D = \frac{kT}{kT_c}, \tag{3}$$

where kT_c is the characteristic energy of the tail. For $T > 170$ K the low-field data approximately fit the linear temperature dependence with $kT_c \approx 23$ meV. However, α_D decreases rapidly to zero below 150 K, which has been attributed to the shift of the mobility edge into the mobility gap and the onset of hopping in the density of localized tail states.[25–28] It is seen in Fig. 2 that these features are considerably changed when the experiments are performed at high fields. It is evident that electric fields greater than 10^5 V/cm significantly affect the carrier thermalization. Measurements of 40 K, where thermal transport can be neglected, are displayed in Fig. 3. Increasing the field from 3×10^5 to 4×10^5 V/cm increases α_D from $\simeq 0.1$ to $\simeq 0.5$. The field-induced characteristics are comparable to temperature-induced features. This is surprising insofar as both parameters act *a priori* very differently on carrier propagation. We have, however, to keep in mind that in disordered materials carrier propagation is dominated by strong scattering

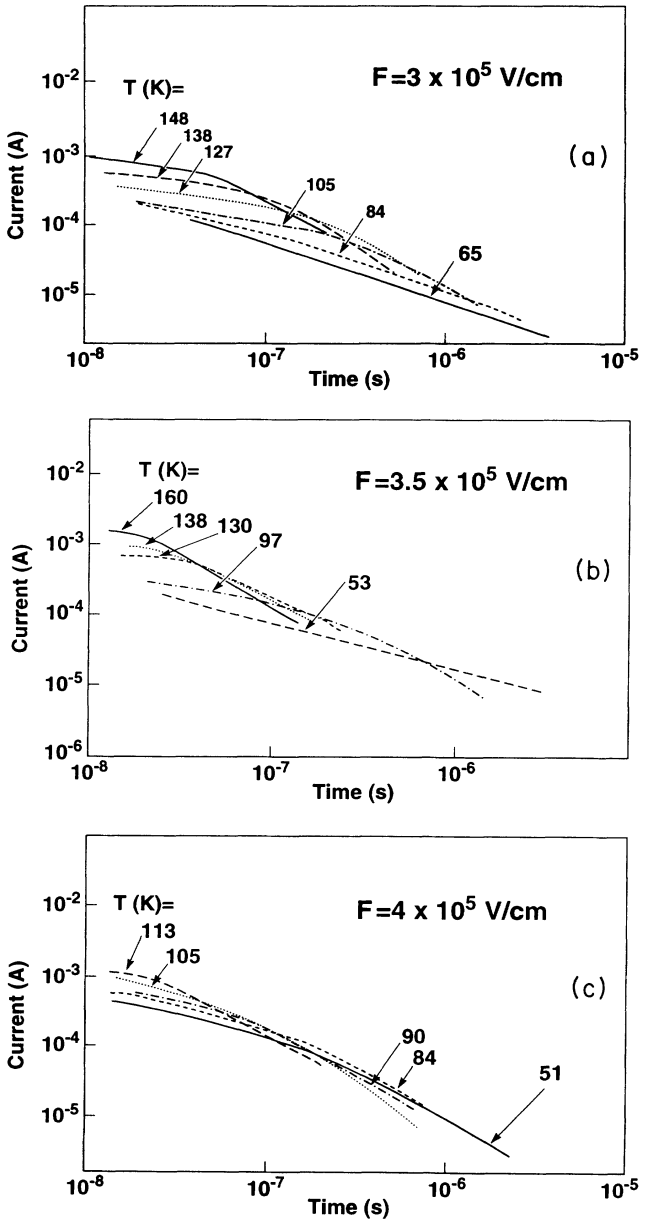

FIG. 1. Temperature-dependent electron current decays measured at electric fields of 3×10^5, 3.5×10^5, and 4×10^5 V/cm on the 10-μm *p-i-n* junction.

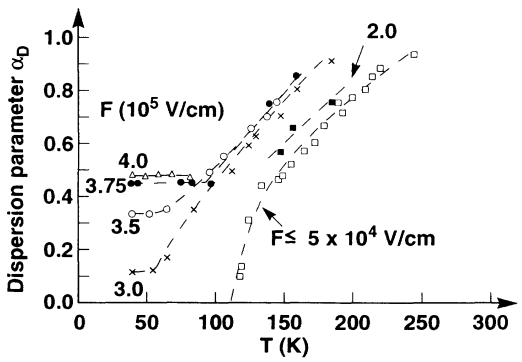

FIG. 2. Dispersion parameter α_D calculated from the power-law time dependence of the transient current decay measured on the 10-μm *p-i-n* junction. For fields $F \leq 5 \times 10^4$ V/cm no field dependence can be detected. Below 150 K the dispersion parameter rapidly approaches zero at low fields.

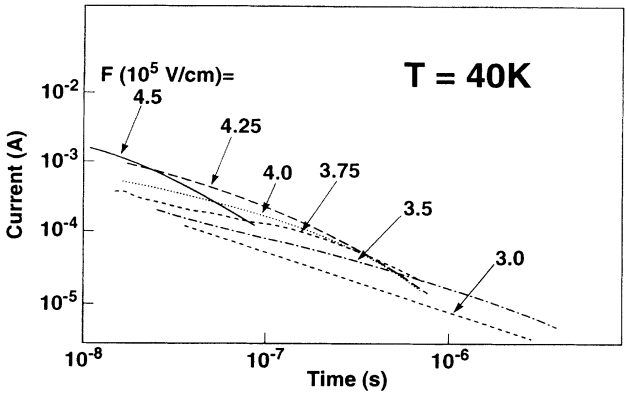

FIG. 3. Field-dependent current decay at $T=40$ K, measured on the 10-μm p-i-n junction.

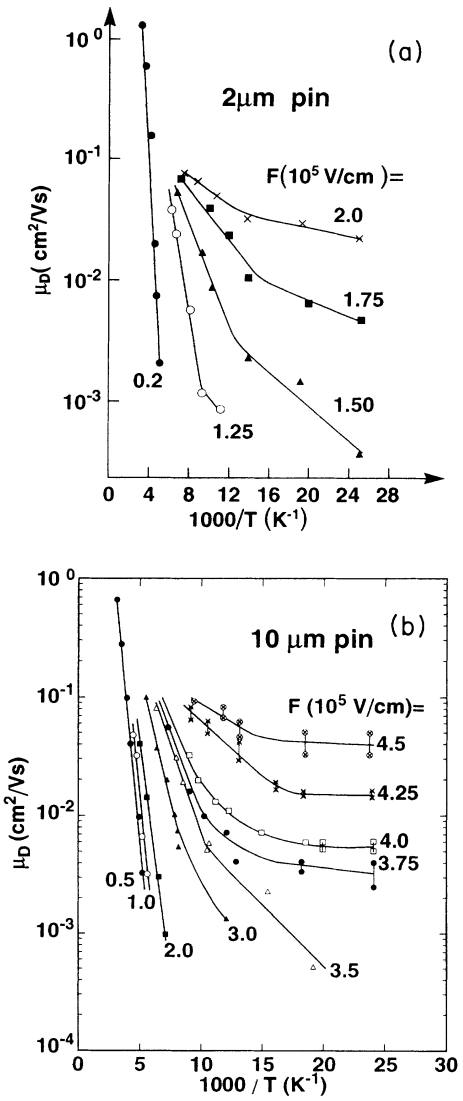

FIG. 4. Temperature- and field-dependent electron drift mobilities measured on the (a) 2-μm and the (b) 10-μm "p-i-n" junction.

processes which restrict energy gain to a minimum and lead to a quasi-isotropic energy emission into the lattice of the amorphous material. To summarize, three characteristic regimes can be distinguished.

(1) A low-field regime where α_D obeys a T/T_c relation for $T>170$ K with $T_c \simeq 260$ K, but α_D rapidly decreases to zero below 150 K.

(2) A regime in the range $90<T<170$ K, where temperature and field effects superimpose. Fields larger than 10^5 V/cm have to be applied to detect a significant field dependence of α_D.

(3) A regime at temperatures below 90 K in which no significant low-field transport is observed. The electron transport increases rapidly at high fields with features analogous to those of higher temperature, low field.

C. Electron drift mobility

Figure 4 shows electron drift mobility μ_D measured as a function of field and temperature on the 2- and 10-μm p-i-n diodes. We define the transit time t_T as the moment at which the current has dropped by 50% relative to the extrapolated pre-transit current decay. The results demonstrate that an increase of μ_D over many orders of magnitude is achieved by varying the temperature and electric field. Field enhancements are predominantly below 100 K and at applied fields above $1-2\times10^5$ V/cm. The drift mobilities are thickness dependent, which is a typical manifestation of the dispersive transport in the presence of high fields. Above $T=100$ K, μ_D is thermally activated with field-dependent energies $E_{\rm act}$ in the range 15–200 meV. $E_{\rm act}$ decreases continuously below 100 K approaching zero at 40 K for the highest applied fields [see Fig. 4(b)]. The disappearance of the activation energy points towards a transport which is entirely controlled by tunneling events rather than thermal excitation. Based on drift mobility data alone it cannot be distinguished whether hopping transport in the tail region or field-induced reemission of electrons back into extended states (or both) is the origin of the high mobilities at 40 K.

D. Charge-collection experiments

The electron drift mobilities can only be deduced from experiments under conditions of almost full charge collection. This has been carefully examined for both samples by charge-collection measurements as displayed in Fig. 5. The measurements have been performed over a constant time window of 10 μs duration. Within this period of time the charge collection approached saturation for high fields typically within 100 ns or dropped below the sensitivity range of the detection system. The absolute number of generated electrons was determined by use of a calibrated c-Si photodiode. Measurements performed with two different laser excitation intensities of 9×10^{-11} C (referred to as 1% L) and 9×10^{-9} C (referred to as 100% L), respectively, reveal the significant change of trapping properties with increasing field. Three characteristic regions of the field-dependent charge collection can be resolved. For $F>2\times10^5$ V/cm (10 μm)

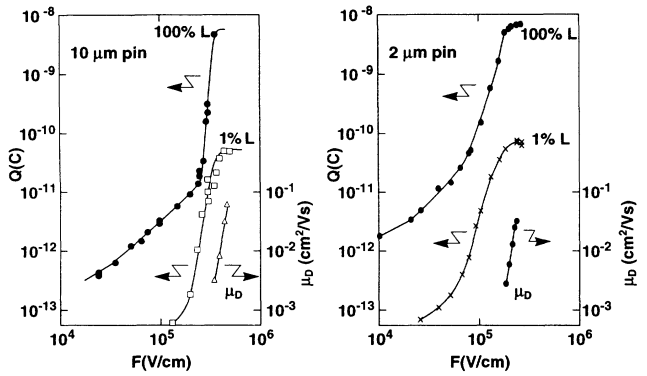

FIG. 5. Charge-collection measurements on the 2- and 10-μm *p-i-n* junction at 40 K recorded for two different laser excitation intensities (referred to as 1% L and 100% L). Also drawn is the field-dependent drift mobility which shows approximately the same superlinear increase as $Q(F)$.

and 6×10^4 V/cm (2 μm) the collection efficiency approaches rapidly a saturation value (region 1) with a superlinear field dependence (region 2) comparable to the increase of the electron mobility (also shown). The number of collected electrons is comparable to the number of generated electrons. We conclude, therefore, that such fields are strong enough to separate electrons and holes in the generation volume, so that recombination is negligible[29] and the transit is dominated by interactions with tail states with waiting times smaller than or equal to the transit time. A calculation of the $\mu\tau$ product defined by the intersection of the extrapolated regions where $Q(F)$ is superlinearly dependent on F and the saturation value results in $\mu\tau\simeq1.2\times10^{-9}$ (2 μm) and $\simeq3\times10^{-9}$ cm^2/V (10 μm). This is about three orders of magnitude larger than values calculated from low-field dc-photoconductivity experiments performed at 40 K.[30] $\mu\tau$ is, however, still $\sim$200–500 times smaller than the room-temperature value which points towards a significant increase of "deep traps" and/or a reduction of the microscopic mobility at the mobility edge.[31] The phrase "deep traps" refers to states which capture but do not reemit electrons within the time frame of the experiment. It is reasonable to assume that at low temperatures, in addition to the defect states, a considerable fraction of the conduction-band tail belongs to this category. The number of collected electrons decreases continuously to lower fields. $Q(F)$ changes to a more weakly dependent function of F in region 3 for $F<2\times10^5$ (10 μm) and $<10^5$ V/cm (2 μm), respectively. Possible reasons are an increasing recombination in the generation volume at lower fields[18,32] and/or hopping down of electrons into deep band-tail states where the waiting time increases considerably.

The experiments reveal the significant influence of electric fields on electron propagation in *a*-Si:H. The field-induced transport enhancement is continuous ranging over orders of magnitude and shows comparable characteristics to thermally induced phenomena. However, a detailed theoretical analysis of high-field carrier hopping in the localized states is needed to distinguish between the possible transport mechanisms of a mobility edge shift, field-induced hopping in the tail, or field-induced reemission back into extended states.

III. ANALYSIS OF TRANSIENT CURRENT DECAY AT HIGH ELECTRIC FIELDS

Transport in disordered materials is a complex problem involving microscopic mechanisms of thermal excitation, diffusion and hopping, distributions of electronic states in energy and space, and macroscopic issues of percolation, etc. A generalized description which offers analytical or numerical solutions of the master equations is still missing. Instead, most approaches have involved considerable approximations, such as those used in the multiple trapping model, to describe an aspect of the general problem. However, this approach has been quite successful in describing dispersive transport in the low-field, intermediate-temperature regime. The following analysis of high-field transport makes similar simplifying assumptions in order to give a tractable calculation.

The purpose of the analysis is to understand the high-field transport data and we therefore focus on the low-temperature regime where field effects are dominant and thermal effects can be neglected ($T\simeq0$ K approach). A detailed justification and the range of validity of this assumption are given in the next section. The freezing in of vibrational energy at low temperatures causes a change of transport features from thermal reemission to phonon-assisted tunneling-dominated propagation of carriers.[25–28] Due to the fact that time-of-flight experiments are performed by exciting electrons optically into the conduction band, where they then thermalize into the density of localized band-tail states, the transport properties are related to events in the shallow tail region where the density of states is high and the transport is reasonably explained by tunneling to nearest accessible states. Variable range hopping typical for low-temperature, low-field transport at the Fermi energy is neglected in this discussion.

Phonon-assisted tunneling in the density of localized states can be discussed either by Monte Carlo calculations (single carrier approach) or by statistical models where the center of charge movement in space and energy is calculated. Despite the shortcomings of idealization, the latter has been successfully applied in the multiple trapping model developed for the interpretation of transport in the medium-temperature, low-field regime. We want to adopt a similar model where carrier propagation is based on nearest-neighbor hopping. Hopping is a dispersive transport process as long as on average carriers lose energy. This is not generally the case at high fields. The dispersive features of the mobility and the dispersion parameter α_D which has been detected experimentally are introduced by the limited probability of carriers being captured ballistically into deep tail states where the increased waiting time in between field-induced reemissions accounts for the dispersive nature. The probability of capture into deep states is linked to the establishment of a transport level at which carriers proceed reasonably fast through the semiconductor. Both nearest-neighbor hopping and ballistic capture are basic assumptions in the transport model that is described below and used for nu-

merical calculations based on computer simulations. It is shown that the field strongly affects the interaction of carriers with localized states. The shallow tail is dominated by rapid energy loss of carriers whereas in the deep tail carriers predominantly gain energy by transitions in field direction. We refer to the energy which separates both parts as the transport energy E_t since carrier propagation takes place predominantly at this level.

The steps in the calculation are as follows.

(1) We first calculate the average transport energy, referred to as the quasimobility edge, under assumptions of nearest-neighbor hopping. The energy is found to depend strongly on the applied field and is the main origin of the field-dependent mobility.

(2) Next the field dependence of the drift mobility is calculated for carriers moving at that transport energy.

(3) Finally, the effects of random trapping into states below the quasimobility edge are included to calculate the drift mobility. Such trapping events are shown to account for the observed dispersion and the absolute magnitude of the mobility.

The calculations are based on the tail state distribution shown in Fig. 6. This density of states (DOS) has been introduced to be typical for the conduction-band tail.[33,34] It is composed of linear and exponential parts. The linearly decreasing tail extends 70 meV from the conduction-band mobility edge E_c [with $g(E_c)=2\times10^{21}$ $\mathrm{cm}^{-3}\,\mathrm{eV}^{-1}$], into the band tail, where it smoothly changes to an exponentially decreasing tail with a characteristic energy $kT_c=25$ meV.

A. The establishment of a transport level

At $t=0$ carriers are excited by a laser flash into the conduction band, initially propagating with the microscopic mobility. The carriers rapidly lose energy ($\sim10^{-12}$–10^{-13} s) by inelastic scattering. After capture into the numerous shallow tail states, further propagation is determined by the tunneling distance between nearest neighbors. There is an energy gain by tunneling in the field direction (referred to as F^+) of an amount $\Delta E_{F^+}=qFr$, where q is the elementary charge and r is the tunneling distance. The number of accessible states is therefore larger than that at zero field which leads to an effective reduction of the average nearest-neighbor distance. Electrons which proceed perpendicular to the field (referred to as F^0) are hopping down in energy just as in the zero-field case, while transitions opposite to the field direction (referred to as F^-) cost the additional energy $\Delta E_{F^-}=-qFr_{F^-}$, which reduces the transition probability in this direction. We assume that transitions take place either perpendicular or parallel to the electric field and neglect transitions which fall out of this definition. This introduces a limited inaccuracy for the regime where the anisotropy is weak. For the case of fields considered in the following this is a minor problem as major parts of the conduction-band tail are dominated either by total anisotropy or isotropy.

As a first step we consider the justification of neglecting thermal excitations. Figure 7 illustrates the competing possibilities of carriers being reemitted thermally or by tunneling to the mobility edge. The temperature regime where field-induced tunneling is dominant can be estimated by comparing the transition probabilities given by

$$\Gamma_{\mathrm{th}}=\nu(E)_{\mathrm{th}}t=\nu_0 t\exp\left[-\frac{\Delta E}{kT}\right] \tag{4}$$

for thermal transition, where ν_0 is the attempt-to-escape frequency $\simeq5\times10^{12}$ s^{-1}, ΔE is the energy from the mobility edge, and the probability for tunneling defined by

$$\Gamma_{F^+}=\nu(E)_{F^+}t=\nu_0 t\exp\left[-\frac{2\Delta r_{F^+}}{\alpha}\right], \tag{5}$$

where Δr_{F^+} is the tunneling distance in the field direction and α is the localization length of an occupied tail state (expected to be in the range 6–10 Å). Inserting the energy gain per tunneling transition ($\Delta E=q\Delta r_{F^+}F$) into Eq. (5) and defining $\Gamma_{\mathrm{th}}\le\Gamma_{F^+}$ gives for the upper limit of the low-temperature regime

$$T_{\max}=\frac{\alpha qF}{2k} \tag{6}$$

in which tunneling dominates over thermal transitions. With values for $\alpha\simeq6$ Å and fields in the range

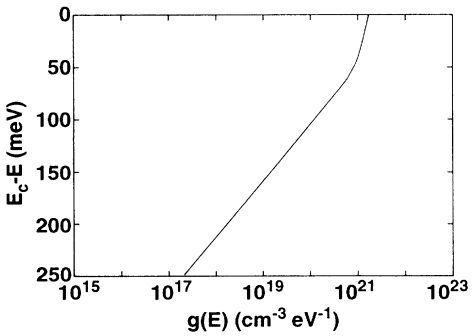

FIG. 6. Hybrid conduction-band tail consisting of a linearly decreasing shallow tail ($E_c-E\le70$ meV) followed by an exponentially decreasing part with the characteristic energy of $kT_c\simeq25$ meV. We assumed a density of states at the transition from extended to localized of 2×10^{21} $\mathrm{cm}^{-3}\,\mathrm{eV}^{-1}$.

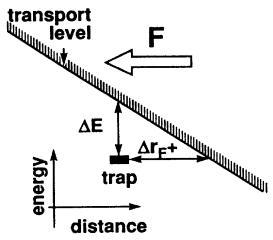

FIG. 7. Schematic picture of a localized state at an energy separation of ΔE from the mobility edge. Due to the presence of the field, a carrier trapped in the localized state can alternatively tunnel to the mobility edge via the path Δr_{F^+} which is equivalent to the energy gain of ΔE.

$10^5 < F < 5\times10^5$ V/cm, the low-temperature regime is given by $35 < T_{max} < 170$ K.

The localization length is a critical parameter, as larger values of α enhance the probability for tunneling and therefore shift the tunneling-dominated regime to higher temperatures. According to Abram and Edwards[35] the decay of a localized wave function depends on energy and can be expressed by

$$\alpha=\alpha_0\left\{\frac{(E_c-E)}{(E_c-E_0)}\right\}^{-\lambda} . \tag{7}$$

Very little is known about the actual numbers for the parameters. Values in the range $5\le\alpha_0\le20$ Å are assumed,[36–38] with an energy dependence[36–39] varying between $0.5\le\lambda\le1$ and $E_c-E_0\simeq0.8$ eV.[36,37] A variety of calculations show that the choice of λ, α_0, and E_c-E_0 sensitively influence the transport properties. Experimental evidence discussed at the end of this section indicates that for shallow tail states α is in the range 6–9 Å. As a first-order approximation we therefore assume $\alpha_0\simeq5$ Å, and $\lambda\simeq0.5$, which are reasonable values from the theoretical point of view, and $(E_c-E_0)\simeq0.8$ eV.

The relative probability for a transition in the field direction (Φ_{F^+}) is given by

$$\Phi_{F^+}=\frac{\Gamma_{F^+}}{\Gamma_{F^+}+\Gamma_{F^-}+\Gamma_{F^0}} , \tag{8}$$

where Γ_{F^0} and Γ_{F^-} are the transition probabilities perpendicular to and opposite to F^+. Φ_{F^-} and Φ_{F^0} are calculated by substituting Γ_{F^+} by Γ_{F^-} and Γ_{F^0}, respectively [see Eq. (5)]. The average nearest-neighbor distance in the F^+ direction for a carrier trapped in a localized state of energy E is determined by

$$r_{F^+}=\left\{\int_0^{E+qFr_{F^+}} g(E^*)dE^*\right\}^{-1/3} , \tag{9}$$

where $g(E)$ is the distribution of localized states. r_{F^-} and r_{F^0} are calculated analogously by changing the integration limits in Eq. (9) from $(E+qFr_{F^+})$ to $(E-qFr_{F^-})$ and to E, respectively.

The calculated field and direction dependences of the nearest-neighbor distance r are shown in Fig. 8, and the related transition probabilities are shown in Fig. 9. For $F=0$, the carrier hopping is isotropic and the transition probability is $\frac{1}{6}$ in r_{F^+} (for example, in x^+ direction) and r_{F^-} (x^- direction), and $\frac{2}{3}$ in r_{F^0} (summation over $y^\pm$ and $z^\pm$). The application of a high field introduces a strong anisotropy in the hopping rates. The deep tail region is completely dominated by transitions in field direction where the carriers gain energy. Transitions perpendicular or opposite to the field occur with reasonable probability only in the shallow tail region. Consequently, the field divides the tail into a high-energy region where hopping down in energy is most probable, and the deep tail region where tunneling transition along field direction dominates and carriers gain energy. Increasing the field

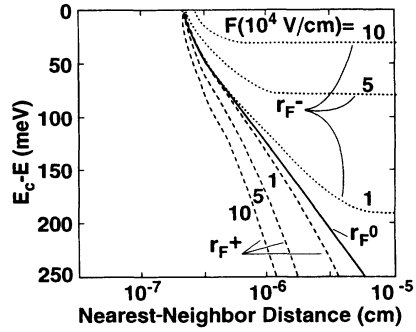

FIG. 8. Applying high electric fields modifies the effective "nearest-neighbor" distance. The distance for transitions in the field direction is shrinking (r_{F^+}), the distance for transitions perpendicular to the field (r_{F^0}) remains unchanged, and the distance for transitions in the opposite field direction increases (r_{F^-}). The figure shows these for electric fields of $F=0$ (full line), 1×10^4, 5×10^4, and 10×10^4 V/cm. Calculated for the DOS shown in Fig. 6.

shrinks the hopping down region and extends the field reemission region.

The thermalization of carriers in energy and space is calculated based on the above model. The energy loss or gain per hop is determined by the transition probabilities. The new energy of a carrier after performing a transition is given from Eq. (9) by

$$E_{new}=E_{old}+\Delta E=E_{old}+\{\Delta E_{r_{F^+}}\Phi_{r_{F^+}}+\Delta E_{r_{F^-}}\Phi_{r_{F^-}}+\Delta E_{r_{F^0}}\Phi_{r_{F^0}}\} , \tag{10}$$

where E_{old} is the energy of the carrier before the transition, $\Delta E_{r_{F^+}}$ is the change in energy in the field direction, and $\Delta E_{r_{F^-}}$ and ΔE_{F^0} are the changes in the opposite and perpendicular field directions, respectively. Tunneling perpendicular to the field changes the energy of carriers

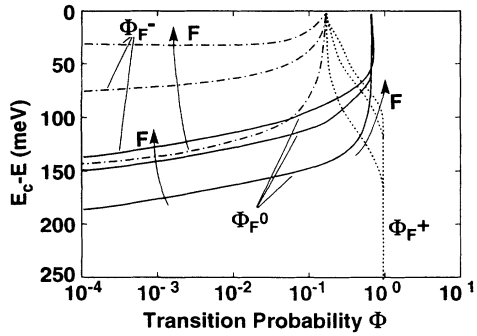

FIG. 9. The transition probabilities in the field direction (Φ_{F^+}, dotted lines), perpendicular to F (Φ_{F^0}, full lines), and opposite to F (Φ_{F^-}, dashed lines) are shown, calculated for the fields $F=1\times10^4$, 5×10^4, and 10×10^4 V/cm for the tail state distribution of Fig. 6. With increasing field, transition in the field direction becomes increasingly dominant even in the shallow tail region.

by the amount

$$|\Delta E_{r_{F^0}}| = \frac{\int_0^{E_{\text{old}}} g(E^*)E^* dE^*}{\int_0^{E_{\text{old}}} g(E^*)dE^*} \tag{11}$$

which for an exponential tail is the characteristic energy $-kT_c$ for each hop. Transitions in the field direction affect the energy by the amount

$$\Delta E_{r_{F^+}} = -\Delta E_{r_{F^0}} + qFr_{F^+} , \tag{12}$$

and transitions opposite to the field by

$$\Delta E_{r_{F^-}} = -\Delta E_{r_{F^0}} - qFr_{F^-} . \tag{13}$$

The waiting time between successive hopping events is given by summing the inverse of the hopping probabilities,

$$t_{\text{hop}}(E) = \nu_0^{-1} \left\{ \exp\left[\frac{-2r_{F^+}(E)}{\alpha(E)} \right] + \exp\left[\frac{-2r_{F^-}(E)}{\alpha(E)} \right] + 4\exp\left[\frac{-2r_{F^0}(E)}{\alpha(E)} \right] \right\}^{-1} . \tag{14}$$

Figure 10 shows the time-dependent hopping down process for carriers starting at $t=0$ in the conduction band at $E=E_c$, for a variety of fields. At zero field, carriers hop down in energy with the speed of the demarcation energy movement as described by Monroe[27] and Silver and Bässler.[28] An applied electric field of a sufficient strength limits the thermalization, based on pure nearest-neighbor hopping. Carriers sink down to the level where the energy loss and gain is balanced, and this is the transport energy E_t. E_t shifts towards the conduction band with increasing field and approaches E_c for $F > 10^6$ V/cm. The establishment of a "transport level" at high fields is comparable to the mobility edge description of the thermal-induced transport.

B. Transient current decay based on nearest-neighbor hopping

It is now necessary to calculate the mobility of carriers in the electric field based on the nearest-neighbor band-tail hopping model, in order to simulate the results of the time-of-flight experiment. The high-field hopping mobility is derived from the Einstein relation[40,41] introducing anisotropic diffusive carrier motion, as follows:

$$\mu_{\text{hop}}(E) = \Phi_{F^+}(E) \left[\frac{q}{kT} \right] \langle r_{F^+}(E) \rangle^2 \times \nu_0 \exp\left[-\frac{2r_{F^+}(E)}{\alpha} \right] . \tag{15}$$

Figure 11 shows μ_{hop} as a function of energy and field. The mobility in the shallow tail is only slightly affected by the field. However, μ_{hop} in the deep tail changes by many orders of magnitude, due to the field. The small variance in the shallow tail region is partly due to the linearly decreasing distribution of tail states (giving a small change in nearest-neighbor distance as a function of energy), and partly due to the energy dependence of the localization length [see Eq. (7)]. Note that at zero field, μ_{hop} is the isotropic mobility introduced by Shapiro and Adler[21] from the discussion of the low-field conductivity.

The drift of the center of charge in the field is described by

$$v(t) = F\mu_{\text{hop}}(t) , \tag{16}$$

where $\mu_{\text{hop}}(t)$ is the hopping mobility related to the time-dependent center of charge energy level, which is displayed in Fig. 10. The average mobility (μ_D) of carriers propagating through a sample of thickness d is defined by

$$\mu_D(F) = \frac{d}{t_T} = t_T^{-1} \int_0^{t_T} v(t)dt , \tag{17}$$

where t_T is the statistical transit time. The results shown in Fig. 12 are calculated for a sample of thickness $d=10$ μm, the tail state distribution of Fig. 6, and other parameters discussed above. The results are compared to the experimentally deduced data measured on the 2- and 10-μm *p-i-n* junctions.

The calculated mobility in Fig. 12 deviates considerably from the experimental data. We performed a variety of calculations in order to fit the data, but failed to

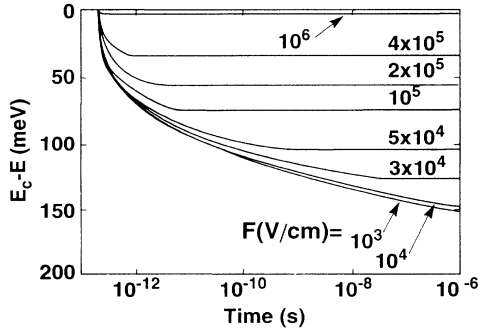

FIG. 10. The time dependence of nearest-neighbor hopping down processes in the presence of electric fields. Carriers approach a minimum energy below which they cannot thermalize. Calculated for the DOS shown in Fig. 6.

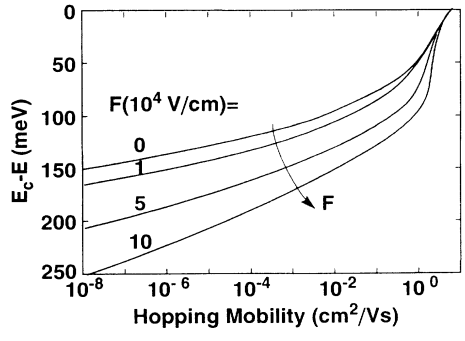

FIG. 11. The hopping mobility in the tail is energy and field dependent. The hopping mobility in the deep tail is increasing over orders of magnitude whereas the changes in the shallow tail are negligible (calculated for the DOS shown in Fig. 6).

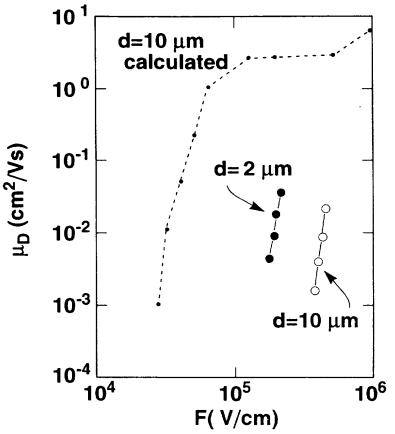

FIG. 12. Drift mobility of electrons calculated for a 10-μm-thick sample (broken line) on the basis of a pure nearest-neighbor hopping transport in the density of localized states as shown in Fig. 6. Also drawn are the experimental results of time-of-flight experiments on *p-i-n* junctions of thicknesses 2 and 10 μm, measured at $T=40$ K.

achieve good agreement with reasonable parameters. Furthermore, the dispersion of μ_D and α_D is not reproduced within the idealized nearest-neighbor hopping model. Electrons approach E_t too rapidly to explain the time dependence and propagate without any further energy loss.

Interaction with deeper tail states is, however, expected to reduce the mobility. A small rate of deep trapping can cause a large change in mobility because the reemission rate from deep traps is very low. This effect is analogous to the role of deep traps in the multiple trapping mechanism. The next section analyzes this extension of the hopping model in detail, and recalculates the drift mobility.

C. High-field dispersive transport

The effect of deep trapping is derived from the formulas introduced by Schmidlin[9] for dispersive transport in the thermally dominated regime. He introduced a simple equation to calculate the statistical transit time of carriers moving through a sample of given thickness and interacting with localized states by ballistical capture and thermal reemission [see Ref. 9, Eq. (82)]. We replace the thermal excitation by field-induced hopping and neglect thermal propagation. This leads to some modifications which are discussed below. We assume ballistical capture into the deep states, which we expect to be a reasonable transition mechanism. The rate of capture is proportional to the hopping velocity of carriers and the number of states passed during transit. For simplicity, we assume a field-independent mobility at E_T, which is reasonable since the mobility at E_T is a weak function of F in the experimental field regime $F>10^5$ V/cm (see for comparison Fig. 12). For fields $F<10^5$ V/cm, the average hopping mobility at E_t and the energetic position of E_T in the tail are strongly field dependent. A discussion of transport in this regime is beyond the scope of this paper.

1. The attempt-to-escape frequency

For low temperatures and high fields we need to modify the conventional multiple trapping equations. The reemission of carriers is dominated by field-induced tunneling of deeply trapped carriers to the transport level as described by Eq. (4). Tunneling the distance Δr_{F+} to the transport level is equivalent to the energy gain $\Delta E=E_c-E=q\Delta r_{F+}F$ (see Fig. 7). Inserting this into Eq. (5) gives[19]

$$\nu(E)=\nu_0(E_T)\exp\left[-\frac{2(E_T-E)}{q\alpha F}\right]. \tag{18}$$

The attempt-to-escape frequency $\nu_0(E_T)$ at the transport level defined by detailed balance is

$$\nu_0(E_T)=\mu_{\rm hop}(E_T)F\sigma N_{t\ \rm eff}, \tag{19}$$

where $N_{t\ \rm eff}$ is the effective density of state and $\mu_{\rm hop}(E_t)F$ is the velocity at the transport energy E_t. Although the hopping mobility is anisotropic it is justified to introduce the hopping mobility in the field direction as the dominant term in the carrier velocity [Eq. (19)] because most of the carriers are moving in direction of F with $\mu_{\rm hop}(E_T)$, and $\mu_{\rm hop}(E_T)$ is also much larger than the hopping mobility perpendicular or opposite to F. This attempt-to-escape frequency is different from the thermal-dominated attempt-to-escape frequency defined by

$$\nu_{0\ \rm th}(E_c)=v_{\rm th}\sigma N_{c\ \rm eff}. \tag{20}$$

The effective density of states at the transport level is

$$N_{\rm eff}=g(E_t)kT \tag{21}$$

which introduces the problem of determining $g(E_t)$ and defining the energy range of states above E_t which are involved in the transport. At low fields the transport level is deep in the tail so that $g(E_t)$ can be orders of magnitude smaller than that at high fields where E_t is in the shallow tail. However, at fields comparable to those applied experimentally ($F>2\times10^5$ V/cm) E_t is in the weakly varying shallow tail region where $g(E_t)$ is comparable to $g(E_c)$ (see Figs. 6 and 10). The transport takes place within a narrow band of states above E_t. The exact energy range of states involved is hard to determine. We therefore use the effective temperature definition[19] as an approximate solution for this problem. $T_{\rm eff}$ at E_t is approximately

$$T_{\rm eff}(E_T)\simeq\frac{\alpha(E_T)qF}{2k} \tag{22}$$

and strongly dependent on the localization length α at E_t and the field. Inserting values $10\le\alpha(E_t)\le20$ Å and an electric field of $F=3\times10^5$ V/cm which is typical for fields used in the experiments results in $170<T_{\rm eff}<340$ K. This is comparable to values assumed in the conventional thermally dominated transport. We conclude therefore that in the high-field regime a major difference in ν_0 should not arise due to significant differences in the effective density of states. However, by detailed balance

the thermal velocity v_{th} is replaced by the product $F\mu_{hop}(E_t)$ which can be significantly smaller than v_{th} and vary with applied field.

2. *Time-of-flight transport at high fields*

The striking equivalence between temperature- and field-induced transport suggests that a modified application of Schmidlin's time-of-flight approach[9] is appropriate. Based on multiple trapping he developed a simple equation in order to calculate the statistical transit time of an ensemble of nonequilibrated carriers moving by an electric field through a semiconductor with localized band-tail states. The transit time is the summation over the time carriers spend in the transport level, which is t_0, plus the summation over all waiting times in localized states below E_t. The capture into deep traps is proportional to the product of the carrier velocity at E_t, the capture cross section (σ), and the number of states [$\Delta Eg(E)$] at a given level E. We replace the continuous DOS by discrete levels with $N_i=\Delta Eg(E_i)$ states where ΔE (we assumed $\Delta E=2.5$ meV) is the energy spacing between each level and $E_i=i\Delta E$. This leads to

$$t_T=t_0\left\{1+\sum_{i}^{}\mu_{hop}(E_T)F\sigma N_i\nu_i^{-1}\right\}, \tag{23}$$

where t_T is the statistical transit time of an ensemble of carriers and ν_i is the reemission frequency of level i. Here i is 0 at E_T and increases with increasing distance from the transport energy. The mean thermal velocity v of Schmidlin's approach has been replaced by ($\mu_{hop}F$). The distance d between front and back contact is covered partly by movement at the transport energy and partly by field-induced tunneling transitions out of deep traps to the transport level,

$$d=t_0\mu_{hop}(E_T)\left\{1+\sum_{i}^{}\sigma N_i\Delta x_i\right\}, \tag{24}$$

where x_i represents the tunneling distance from trap i to the transport level.

Transport in a DOS distribution as shown in Fig. 6 is determined by capture of carriers into and reemission out of the numerous shallow traps close to the transport energy. The fewer deeper states have a smaller capture probability. The summation in Eqs. (23) and (24) is carried out therefore only over tail states with a high capture probability. Marshall, Berkin, and Main[42] and Silver, Snow, and Adler[43] discussed this problem in detail and presented an equation to determine the summation limit. They define deep traps as states which in total have a capture rate less than one per carrier transit. This is equivalent to

$$\mu_{hop}(E_T)Ft_0\sum_{i+1}^{\infty}\sigma g_i\Delta E\le 1\ . \tag{25}$$

With Eqs. (23)–(25) the statistical transit time t_T and the mobility μ_D of an ensemble of nonequilibrated carriers in the presence of high fields and low temperature are calculated self-consistently. Parameters which enter the equations are the distribution of localized states, the capture cross section of traps, the hopping mobility at E_t, the attempt-to-escape frequency, the transport level energy, and the localization length. To calculate fits to the experimental data we introduce the DOS as shown in Fig. 6 and the capture cross section of 10^{-15} cm^2 independent of energy.[44] We assume $\mu_{hop}(E_t)$ and E_t to be field independent, based on considerations presented in Sec. III A.

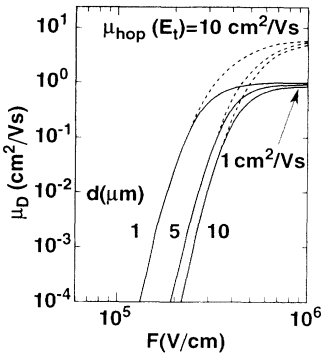

FIG. 13. The field-induced transport is thickness dependent (calculated for $d=1$, 5, and 10 μm) turning over at high fields to the maximum hopping mobilities at the transport level which we assumed to be $\mu_{hop}=1$ (full line) and 10 cm^2/V s (dashed line), respectively.

Figure 13 shows the calculated drift mobility as a function of F and sample thickness for $\mu_{hop}(E_t)=1$ and 10 cm^2/V s, respectively. $\mu_D(F)$ is increasing over orders of magnitude with increasing F, turning over at high fields to a saturation value which is given by $\mu_{hop}(E_t)$. μ_D is also thickness dependent, which indicates dispersive transport in the presence of high fields. This feature can be explained analogously to the thermal-induced transport. High enough fields keep the center of charge in the transport states where carriers propagate with the mobility at E_t. Lowering the field causes a drop of the center of charge below the transport level which is field dependent and hence dispersive. The increase of μ_D as a function of F is not specifically dependent on the mobility at E_t, as shown in Fig. 13 with $\mu_{hop}(E_t)$ assumed to be 1–10 cm^2/V s, respectively. It demonstrates that neglecting the field dependence of $\mu_{hop}(E_t)$ is a reasonable approach.

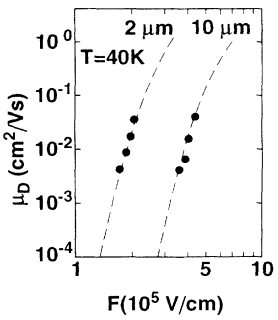

FIG. 14. Calculated fit to the experimental data measured at $T=40$ K based on Eqs. (21)–(23) and the DOS shown in Fig. 6.

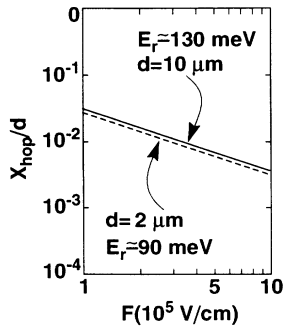

FIG. 15. Although the reemission of deep trapped electrons is based on field-enhanced tunneling back to the transport levels, the distance carriers proceed by the reemission is small compared to the distance they hop at the transport level. E_r is the deepest encountered trap state below the transport level.

Figure 14 shows calculated fits to the drift mobility measured on the 2- and 10-μm *p-i-n* junctions at 40 K with the DOS as shown in Fig. 6, capture cross section $\sigma=10^{-15}$ cm^2/V s, attempt-to-escape frequency $\nu_0 \simeq 3\times10^{12}$ ($d=10$ μm) and 5×10^{12} s^{-1} ($d=2$ μm), respectively, and an energy-independent localization length $\alpha\simeq5$ ($d=10$ μm) and 7 Å ($d=2$ μm), respectively. The values indicate that the transport level at high fields is in the shallow tail close to E_c. A considerable drop of E_t deep into the tail cannot be derived from this calculation. The attempt-to-escape frequency deduced from the fits is close to the value determined from time-of-flight experiments in the thermally dominated regime[45] (5×10^{12} s^{-1}). The interpretation of the slight differences in α and ν_0 is beyond the accuracy of this treatment.

Figure 15 displays the distance carriers cover by tunneling from deep traps to the transport level ($x_{\rm hop}$) relative to the sample thickness. In both cases $x_{\rm hop}$ is surprisingly small, falling below 1% of the total distance and decreasing with increasing field. The deepest levels encountered in the transport are $\simeq$90 and $\simeq$130 meV for the 2- and 10-μm samples, respectively.

In general we achieved reasonable agreement between experimental data and theoretical calculations with parameters conventionally assumed for electron transport in *a*-Si:H.

3. Time-dependent demarcation energy

The time dependence of the demarcation energy is defined by the condition

$$\nu(E_D)t=1=\nu_0 t\exp\left\{-\frac{2E_D(t)}{q\alpha F}\right\}, \tag{26}$$

which introduces the assumption that a state at energy E is equilibrated with the transport levels after at least one reemission event in the time period t.[46] This leads to

$$E_D(t)=\frac{q\alpha F}{2}\ln(\nu_0 t)\ . \tag{27}$$

Based on this equation we can estimate the deepest trap encountered below the transport level, by inserting transit times measured for the 2- and 10-μm samples. For $\alpha\simeq7$ Å and $\nu_0\simeq5\times10^{12}$ s^{-1} the results are $E_D(t_T)\simeq75$ (2 μm), and 120 meV (10 μm), respectively, which are in reasonable agreement with results deduced by Eq. (25) where the deepest encountered state below the transport level has been calculated to be 90 meV for the 2-μm and 130 meV for the 10-μm sample.

4. Field-dependent dispersion

In this section we assume an energy-independent localization length. This is acceptable as long as the interaction of carriers is dominated by deep tail states where even for an energy dependence of the localization length α is weakly varying with E. Time-of-flight transients with time windows $t>10^{-9}$ s have to be related to electron interactions with those states as shown in Sec. III B. If we further assume carrier interactions with an approximate exponential tail state distribution which is reasonable as shown above we can modify the well-known transport equation of the transient current decay[46,47] in a simple way. Instead of thermal reemission we introduce field-induced reemission which results in

$$I(t)\simeq G_0\left\{\frac{\mu_{\rm hop}(E_T)F}{d}\right\}\Psi(1-\alpha_D)\frac{\sin^2(\alpha_D\pi)}{\pi}\times\{\nu_0 t\}^{-(1-\alpha_D)}, \tag{28}$$

where G_0 is the generation rate and Ψ is the gamma function. The field-dependent transient current decay is dispersive with a dispersion parameter α_D defined by

$$\alpha_D=\frac{q\alpha F}{2kT_c}\ . \tag{29}$$

α_D depends on F which has been experimentally detected as shown in Fig. 2 and on the characteristic energy kT_c of the exponential tail state distribution. We can estimate the localization length α by introducing the characteristic energy kT_c calculated in Sec. III B and taking the α_D data shown in Fig. 2 ($T=40$ K). This gives $5<\alpha<6$ Å which is in reasonable agreement with values discussed above. We also can estimate the transition from dispersive to nondispersive transport ($\alpha_D=1$) based on Eq. (29) which should occur at $F\simeq8\times10^5$ V/cm for parameters $kT_c=25$ meV and $\alpha\simeq6$ Å.

IV. THE ANALOGY BETWEEN TEMPERATURE AND ELECTRIC FIELD

The striking analogy between field- and temperature-induced transport suggests the conclusion that the electric field acts like a temperature. Shklovskii and coworkers[19] introduced a theoretical argument that for (1) an established transport level, (2) direct field-induced reemission of deep trapped carriers to this level, and (3) a constant localization length α, the electric field can be transformed into an effective temperature given by Eq. (1). In the previous sections we have shown that the introduction of a transport level and direct reemission reasonably well explains the field dependence of the electron drift mobility. From the theoretical point of view an

energy-independent localization length seems to be an unrealistic assumption, however, due to (1) the interaction of electrons with a limited part of the conduction-band tail and (2) the transport level in the density of localized states, the variation of α can be assumed to be small. These arguments also indicate that the presented data cannot be applied to justify the concept of the "effective temperature approach" in general. We want to apply the effective temperature definition to estimate the localization length of trapped electrons in the shallow tail states based on the drift mobility and dispersion parameter data shown in Figs. 2 and 4.

Shklovskii and co-workers[19] proposed a simple way to determine the effective temperature by comparing transport data measured at low fields in the temperature-dominated regime with high-field data measured at low temperatures. This leads to the equation for drift mobility comparisons,

$$\mu_D(T_{\text{eff}},F=0)=\mu_D(T,F)\ , \tag{30}$$

and for the dispersion parameter comparisons,

$$\alpha_D(T_{\text{eff}},F=0)=\alpha_D(T,F)\ , \tag{31}$$

where the zero-field μ_D data have in fact been measured at $F=5\times10^4$ V/cm. Results are displayed in Fig. 16. T_{eff} calculated from drift mobility comparisons measured at 40 K (10 μm) is approximately linearly dependent on F. A fit of Eq. (1) to the data [dashed line in Fig. 16(a)] results in a localization length $\alpha\simeq9$ Å. The field-induced transport at 40 K reproduces features which are comparable to data measured in the temperature range $200<T<250$ K at low fields [see Fig. 16(a)]. A comparison of the dispersion parameter values [see Fig. 16(c)], however, results in smaller T_{eff} values of $120<T_{\text{eff}}<150$ K. A discrepancy of ~50 K arises which leads to a slightly smaller value for the localization length $\alpha\simeq6$ Å. The evaluation of α_D is, however, very critical and only of limited accuracy (±0.1).

Up to now the discussion has focused on either field- or temperature-dominated transport. There is, however, a broad transition region where both coexist. At the higher temperatures the dominance of the field vanishes in favor of thermally dominated transport. The onset of the transition depends on field strength and takes place gradually. Several suggestions have been made concerning a substitution of field and temperature into an effective temperature,[19,20,48] an effort which we want to discuss briefly on the basis of the data shown in Figs. 2 and 4 and Eqs. (30) and (31). The result is shown in Figs. 16(b) and 16(c). T_{eff} is a nonlinear function of T which can be fitted [full lines in Figs. 16(b) and 16(c)] with reasonable agreement by[48]

$$T_{\text{eff}}^2=T^2+\left\{\frac{q\alpha F}{2k}\right\}^2\ . \tag{32}$$

Equation (32) is derived empirically from Monte Carlo calculations; a theoretical argument is still missing. A fit of Eq. (32) to the T_{eff} data calculated from drift mobility comparisons achieves reasonable agreement for a localization length $\alpha\simeq9$ Å. The fit to T_{eff} values determined by the dispersion parameter comparison results in a slightly smaller value $\alpha\simeq6$ Å. The values of α deduced from this procedure are comparable to those determined by the simulation of high-field time-of-flight experiments based on Eqs. (23)–(25). We conclude therefore that the introduction of T_{eff} as a substitution for temperature and field reasonably well describes the overall transport features measured by time-of-flight experiments. A linear

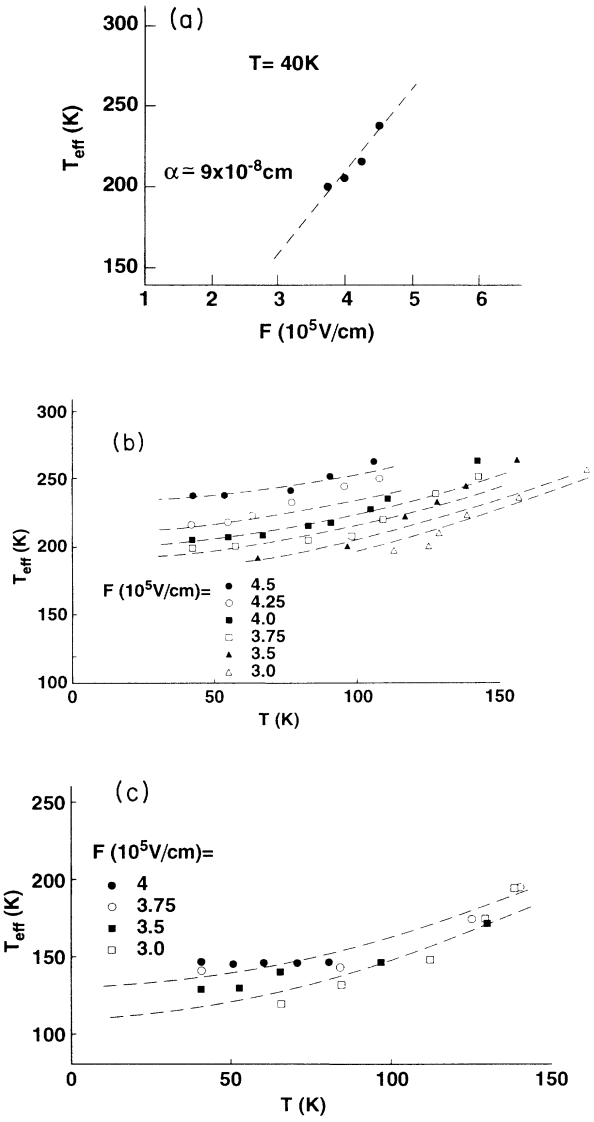

FIG. 16. (a) Calculated fit of Eq. (1) (dashed line) to the T_{eff} data deduced by Eq. (30) from the data shown in Fig. 4(b). This results in a localization length of $\alpha\simeq9$ Å. (b) T_{eff} as a function of the temperature for different electric fields. Dashed lines represent a fit calculated by Eq. (32) ($\alpha\simeq9$ Å) to the data. T_{eff} has been determined by comparing the field- and temperature-dependent mobility data as displayed in Fig. 4(b) by the formalism described in Eq. (30). (c) T_{eff} as a function of the temperature and field calculated by comparing the dispersion parameter values as shown in Fig. 2 and the formalism described by Eq. (31). Dashed line represents the calculated fit of Eq. (32) to the data of $F=3\times10^5$ and 4×10^5 V/cm which gives a localization length of $\alpha\simeq6$ Å.

superposition[17] of temperature and field or the definition $T_{\text{eff}}=\max(T,q\alpha F/2)$ as proposed by Esipov[20] leads to a strong divergence between fit and data.

It is important to note that recently performed Monte Carlo simulations[22] indicate that for a given high field two regimes—the shallow and the deep tail—with different T_{eff} values exist. Following these arguments the effective temperatures deduced from time-of-flight experiments are then related to specific transport properties of the shallow tail regime where the above-mentioned preconditions—establishment of a transport level E_T, direct field-induced reemission to E_T, negligible variation of the localization length—for the introduction of an effective temperature (T_{eff}) are fulfilled. The definition of T_{eff} as a universal quantity which would enable a general discussion of transport properties in a-Si:H, however, cannot be confirmed. Time-of-flight data are related to a much too narrow energy regime to argue for or against a universal validity of the effective temperature approach.

V. CONCLUSIONS AND SUMMARY

Time-of-flight experiments performed on p-i-n junctions of different thicknesses reveal surprisingly high electron mobilities and $\mu\tau$ products at lowest temperatures in the presence of high electric fields. The drift mobility is superlinearly dependent on the electric field with values comparable to data deduced in the temperature-dominated regime. We also detect a thickness dependence which indicates the dispersive nature of high-field transport. The thermalization of electrons at high fields of $F>10^5$ V/cm is slowed down which can be detected over a broad temperature regime. With increasing temperature the transport properties change gradually from field to thermal domination.

Charge-collection experiments performed at $T=40$ K reveal $Q(F)$ to be superlinearly dependent on F, comparable to the superlinear increase of the mobility. At sufficiently high fields the collection efficiency is surprisingly high. About 90% of the number of generated electrons can be collected which results in a $\mu\tau$ product of $\sim 10^{-9}$ cm^2/V s.

The low-temperature experiments demonstrate that a-Si:H switches with increasing field continuously from nonconducting to highly conducting. The features of electron transport at high fields are comparable to thermally induced transport.

Carrier propagation at low temperatures in a high density of localized states is dominated by phonon-assisted nearest-neighbor hopping. Based on statistical arguments, the isotropic diffusive movement of carriers changes considerably in the presence of high fields. In the shallow tail, carriers propagate with a field-dependent hopping mobility, sinking rapidly to the energy level where energy loss and gain are balanced. We introduce this energy level as a quasimobility edge, shifting with increasing F closer to the extended states. Electrons are trapped in states below the mobility edge by ballistic capture and reemitted back into the transport states by field-induced tunneling. The increasing probability of deep trapping with increasing transit time causes the dispersive nature of field-induced transport manifested by the experimentally detected thickness dependence of μ_D and the field dependence of α_D. The introduced model is in general comparable to the multiple trapping model with the modification of field- instead of thermal-induced reemission. The time-dependent equilibration at high field can be calculated by a demarcation energy which is governed by the field, the localization length, and the attempt-to-escape frequency.

The introduced model leads to reasonable agreement with experimental data by assuming well-established parameters for the capture cross section of traps ($\simeq 10^{-15}$ cm^{-2}), the attempt-to-escape frequency [$\simeq(3-5)\times 10^{12}$ s^{-1}], and the localization length ($5\leq\alpha\leq 9$ Å). We have performed the calculations based on a hybrid conduction-band tail composed of linear and exponential parts. The linearly decreasing tail extends 70 meV from the conduction-band mobility edge E_c [with $g(E_c)\simeq 2\times 10^{21}$ cm^{-3} eV], into the band tail, where it smoothly changes to an exponentially decreasing tail with a characteristic energy $kT_c=25$ meV.

The calculations show that for fields applied in time-of-flight (TOF) experiments transport takes place in the shallow tail regime ($E_c-E_T<70$ meV). The deepest trap levels encountered are $\simeq 90$ (2 μm) and $\simeq 130$ meV (10 μm) below the transport level E_T, respectively. Electrons which are deeper trapped are effectively frozen in for time-of-flight experiments.

Based on the calculations presented above we can predict the transition from dispersive to nondispersive transport for fields $F>8\times 10^5$ V/cm where electrons are field-induced reemitted into the extended states of the conduction band.

The surprising analogy between field- and thermal-induced transport supports the argument which introduces an effective temperature as a substitute for the field. The procedure for the determination of T_{eff} introduced by Shklovskii and co-workers[19] leads to reasonable values for the localization length α which is $\alpha\simeq 9$ Å based on drift mobility data and $\alpha\simeq 6$ Å calculated from dispersion parameter data. The introduction of the universal quantity T_{eff} as a substitution for temperature and field reasonably well describes the time-of-flight data. However, the presented data cannot be used to justify the concept of the "effective temperature approach" in general as a too narrow tail state regime is involved in time-of-flight transport.

ACKNOWLEDGMENTS

The work was partially supported by the National Renewable Energy Laboratory. One of the authors (C.E.N.) is pleased to acknowledge partial support from the Alexander von Humboldt Stiftung, Federal Republic of Germany.

[1]R. C. Chittick, J. H. Alexander, and H. F. Sterling, J. Electrochem. Soc. **116**, 77 (1969).
[2]W. E. Spear and P. G. LeComber, Solid State Commun. **17**, 1193 (1975).
[3]W. E. Spear, in *Amorphous Silicon and Related Materials,* edited by H. Fritzsche (World Scientific, Singapore, 1989), p. 721.
[4]J. M. Marshall, R. A. Street, and M. J. Thompson, Philos. Mag. B **54**, 51 (1986).
[5]T. Tiedje, J. M. Cebulka, D. L. Mord, and B. Abeles, Phys. Rev. Lett. **46**, 1425 (1981).
[6]C. E. Nebel and G. H. Bauer, Philos. Mag. B **59**, 463 (1989).
[7]C. E. Nebel, G. H. Bauer, M. Gorn, and P. Lechner (unpublished).
[8]J. M. Marshall, R. A. Street, M. J. Thompson, and W. B. Jackson, Philos. Mag. B **57**, 387 (1988).
[9]F. W. Schmidlin, Phys. Rev. B **16**, 2362 (1977).
[10]N. F. Mott, Philos. Mag. B **51**, 19 (1985).
[11]R. I. Devlen, J. Tauc, and E. A. Schiff, J. Non-Cryst. Solids **114**, 567 (1989).
[12]H. Antoniadis and E. A. Schiff, Phys. Rev. B **43**, 13 957 (1991).
[13]G. Juska, G. Jukonis, and J. Kocka, J. Non-Cryst. Solids **114**, 354 (1989).
[14]J. Kocka, C. E. Nebel, G. H. Bauer, O. Klima, Y. Xiao, E. Sipek, and G. Juska, in *The Physics of Semiconductors,* edited by E. M. Anastassakis and J. D. Joannopoulos (World Scientific, Singapore, 1990), p. 2059.
[15]C. E. Nebel and J. Kocka, in *Amorphous Silicon Technology—1991,* edited by Arun Madan *et al.* (Materials Research Society, Pittsburgh, 1991), p. 563.
[16]S. Imao, S. Nakajima, J.-I. Nakata, R. Hattori, J. Shirafuji, and Y. Inuishi, Jpn. J. Appl. Phys. Lett. **30**, 1227 (1991).
[17]C. E. Nebel, J. Non-Cryst. Solids **137&138**, 395 (1991).
[18]R. Stachowitz, W. Fuhs, and K. Jahn, Philos. Mag. B **62**, 5 (1990).
[19]B. I. Shklovskii, E. I. Levin, H. Fritzsche, and S. D. Baranovskii, in *Advances in Disordered Semiconductors,* edited by H. Fritzsche (World Scientific, Singapore, 1990), Vol. 3, p. 161.
[20]S. E. Esipov, Phys. Rev. B **44**, 7930 (1991).
[21]F. R. Shapiro and D. Adler, J. Non-Cryst. Solids **74**, 189 (1985).
[22]R. Schumacher, Ph.D. thesis, Universität Marburg, 1991.
[23]T. Tiedje, in *Hydrogenated Amorphous Silicon Part C,* edited by J. I. Pankove, Semiconductors and Semimetals Vol. 21 (Academic, New York, 1984), p. 207.
[24]J. M. Marshall and D. Allen, Philos. Mag. B **40**, 71 (1979).
[25]C. E. Nebel, H. C. Weller, and G. H. Bauer, in *Amorphous Silicon Technology—1990,* edited by Arun Madan *et al.* (Materials Research Society, Pittsburgh, 1990), p. 151.
[26]T. Tiedje, in *Proceedings of the International Workshop on Amorphous Semiconductors,* edited by H. Fritzsche, D.-X. Han, and C. C. Tsai (World Scientific, Singapore, 1987), p. 113.
[27]D. Monroe, Phys. Rev. Lett. **54**, 146 (1985).
[28]M. Silver and H. Bässler, Philos. Mag. Lett. **56**, 109 (1987).
[29]G. Juska, K. Arlauska, O. Klima, and J. Kocka, J. Non-Cryst. Solids (to be published).
[30]H. Fritzsche, J. Non-Cryst. Solids **114**, 1 (1989).
[31]J. Kocka, C. E. Nebel, and C.-D. Abel, Philos. Mag. B **63**, 221 (1991).
[32]K. Jahn, W. Fuhs, and K. Pierz, J. Non-Cryst. Solids **114**, 307 (1989).
[33]R. A. Street, J. Kakalios, and M. Hack, Phys. Rev. B **38**, 5630 (1988).
[34]R. A. Street, M. Hack, and W. B. Jackson, Phys. Rev. B **37**, 4209 (1988).
[35]R. A. Abram and S. Edwards, J. Phys. C **5**, 1183 (1972).
[36]M. Kemp and M. Silver, Philos. Mag. B **63**, 437 (1991).
[37]W. E. Spear and C. S. Cloude, Philos. Mag. B **58**, 467 (1988).
[38]M. Stutzmann, J. Non-Cryst. Solids **97&98**, 105 (1987).
[39]V. Heuckeroth, H. Overhof, R. Schumacher, and P. Thomas, Philos. Mag. B **63**, 193 (1991).
[40]H. Kamimura and H. Aoki, in *The Physics of Interacting Electrons in Disordered Systems* (Clarendon, Oxford, 1989).
[41]R. A. Street, in *Hydrogenated Amorphous Silicon,* edited by R. W. Cahn, E. A. Davis, I. M. Ward, Cambridge Solid State Science Series (Cambridge University Press, Cambridge, England, 1991).
[42]J. M. Marshall, J. Berkin, and C. Main, Philos. Mag. B **56**, 641 (1987).
[43]M. Silver, E. Snow, and D. Adler, J. Appl. Phys. **59**, 3503 (1986).
[44]R. A. Street, J. Zesch, and M. J. Thompson, Appl. Phys. Lett. **43**, 672 (1983).
[45]C. E. Nebel, Ph.D. thesis, Universität Stuttgart, 1990.
[46]J. Orenstein, M. A. Kastner, and V. Vaninov, Philos. Mag. B **46**, 23 (1982).
[47]T. Tiedje, in *Hydrogenated Amorphous Silicon II,* edited by J. D. Joanopoulos and G. Lucovsky (Springer-Verlag, Berlin, 1984), p. 261.
[48]B. Shklovskii (private communication).